Available online at www.sciencedirect.com
SCIENCE DIRECT
Journal of Power Sources 150 (2005) 247–254
JOURNAL OF POWER SOURCES
www.elsevier.com/locate/jpowsour

Effect of annealing treatment on structure and electrochemical properties of $La_{0.67}Mg_{0.33}Ni_{2.5}Co_{0.5}$ alloy electrodes

Faliang Zhang [a], Yongchun Luo [b,*], Jiangping Chen [a], Ruxu Yan [a], Long Kang [a], Jianhong Chen [a]

[a] *Department of Materials Science and Engineer, Lanzhou University of Technology, Lanzhou 730050, PR China*
[b] *State Key Laboratory of Advanced Non-Ferrous Materials, Lanzhou University of Technology, Lanzhou 730050, PR China*

Received 15 November 2004; received in revised form 7 February 2005; accepted 26 February 2005
Available online 2 April 2005

Abstract

$La_{0.67}Mg_{0.33}Ni_{2.5}Co_{0.5}$ alloys were prepared by induction melting followed by different annealing treatments (1023, 1073, 1123 and 1173 K) for 24 h. Alloy structure and electrochemical properties of different annealed alloys have been studied systematically by X-ray diffraction (XRD), scanning electron microscope (SEM) and electrochemical experiments. Alloy structure analyses show that all of the alloys consisted of complex phases such as (La, Mg)(Ni, Co)$_3$ phase ($PuNi_3$-type, SG: R-3 m), (La, Mg)$_2$(Ni, Co)$_7$ phase (Ce_2Ni_7-type, SG: $P6_3/mmc$), LaMg(Ni, Co)$_4$ phase ($MgCu_4Sn$-type, SG: F-4 3 m) and La(Ni, Co)$_5$ phase ($CaCu_5$-type, SG:P6/mmm). One thousand one hundred and twenty-three kelvin benefited formation of (La, Mg)(Ni, Co)$_3$ phase best. Main phase in alloy became (La, Mg)$_2$(Ni, Co)$_7$ phase at 1173 K annealing treatment. Electrochemical experiments show that absorption/desorption plateau became flatter and wider after annealing treatment, that all of the alloy electrodes exhibited good activation characteristics, that annealing treatment improved discharge capacities of alloy electrodes from 315 mAh g^{-1} (as-cast) to 402.5 mAh g^{-1} (1173 K). At the same time, cyclic stability of alloy electrodes was also improved with rise of annealing temperature, especially for alloy electrode (S_{70} = 92.9%) with main phase (La, Mg)$_2$(Ni, Co)$_7$ at 1173 K. As (La, Mg)(Ni, Co)$_3$ phase in alloys increased, high rate dischargeability characteristics were deteriorated. However, alloy electrode with main phase (La, Mg)$_2$(Ni, Co)$_7$ exhibited the best kinetic characteristics. All experiments imply that alloy electrode with main phase (La, Mg)$_2$(Ni, Co)$_7$ possessed excellent overall electrochemical properties.

Keywords: Hydrogen storage alloy; Ni/MH battery; Alloy structure; Electrochemical properties

1. Introduction

Hydrogen storage alloys have been attached more and more importance to application and research with "Hydrogen Energy" put forward [1]. Rare-earth-based AB_5-type alloy and Zr-based laves phase alloy have been commercialized successfully as Ni/MH secondary cell negative materials [2,3], but low capacity of AB_5-type alloy electrodes and difficult activation characteristics of laves phase alloy electrodes limit the extensive application [4,5]. Recently, La–Mg–Ni ternary $PuNi_3$-type alloys have been studied extensively due to its higher discharge capacity and excellent activation properties [6–9]. But the cycle stability of alloy electrodes is poor because of big ratio of cell volume expansion and corrosion of La element and Mg element in charge/discharge process [10]. Moreover, the cyclic stability has not been improved effectively until now by alloying with different transition family elements [11–16]. In contrast, annealing treatment gives rise to more important influence on cycle stability of alloy electrodes. For example, Pan et al. [17] found that the cycle stability of $La_{0.67}Mg_{0.33}Ni_{2.5}Co_{0.5}$ alloy electrodes was improved obviously by annealing treatment at 1223 K, but the investigation in more details about the annealed alloy structure and electrochemical properties was not reported later. On the other hand, Kohno et al. [18] once investi-

* Corresponding author. Tel.: +86 931 280 8140; fax: +86 931 280 6962.
E-mail address: luoyc@lut.cn (Y. Luo).

0378-7753/$ – see front matter © 2005 Elsevier B.V. All rights reserved.
doi:10.1016/j.jpowsour.2005.02.031

gated the hydrogen storage properties of ternary system alloys: La_2MgNi_9, $La_5Mg_2Ni_{23}$, La_3MgNi_{14}, and found that $La_{0.7}Mg_{0.3}Ni_{2.8}Co_{0.5}$ alloy electrode exhibited perfect cyclic stability during 30 times charge/discharge cycles when compared to $MmNi_{4.0}Mn_{0.3}Al_{0.3}Co_{0.4}$ alloy electrode. But it is very regretful that the principle was not reported detailedly. In view of the research status of La–Mg–Ni ternary $PuNi_3$-type alloy, we designed the $La_{0.67}Mg_{0.33}Ni_{2.5}Co_{0.5}$ alloy and studied the structure and electrochemical properties of different annealing treatment alloys systematically.

2. Experiment

$La_{0.67}Mg_{0.33}Ni_{2.5}Co_{0.5}$ hydrogen storage alloy was prepared by induction melting at 0.4 Mpa Ar atmosphere followed by annealing treatment at 1023, 1073, 1123 and 1173 K, respectively, for 24 h. Due to the high vapor pressure of Mg element, an appropriate excess of Mg element was necessary. The purity of all elements was above 99 wt.%.

The annealed alloys were crushed mechanically into powder (<38 μm) for X-ray diffraction (XRD) measurements and powder from 54 to 61 μm for electrode test. XRD measurements were performed on a Rigaku D/max-2400 diffractometer with Cu radiation and a power of 40 kV × 100 mA. The patterns were recorded over the range from 8° to 110° in 2θ by step of 0.02°. Then the collected data were analyzed by the Rietveld method [19] using Fullprof 2K software [20] to get the lattice parameters and phase abundance.

The microscopic structure and the composition for annealed alloys were examined by scanning electron microscope (SEM) with energy dispersive spectroscopy (EDS) on a JSM-5000LV instrument. The Mg content in alloys was determined by atom absorption spectrum and the examination was performed on WFX-1D instrument with specified wavelength (285.2 nm) and slot (0.1 nm).

Alloy electrodes were prepared by cold pressing the mixture of alloy power and carbonyl nickel power at the weight ratio of 1:3 under 800 MPa pressure to form a pellet of 10 mm in diameter. Electrochemical measurements were performed at 293 K in a standard open tri-electrode electrolysis cell consisting of alloy electrode, a sintered $Ni(OH)_2$/NiOOH anode and a Hg/HgO reference electrode immersed in 6 M KOH electrolyte. Each electrode was discharged to cut-off potential −0.6 V versus Hg/HgO reference electrode. Electrodes were charged/discharged at 100 mA g^{-1} when activated; Electrodes were charged/discharged at 300 mA g^{-1} when examined for cyclic stability. Because of low hydrogen absorption/desorption plateau for La–Mg–Ni alloy system [10], a self-discharge problem can be ignored if the time for testing of electrodes is not very long [21]. Therefore, *P–C* isotherms could be determined by electrochemical method according to the Nernst equation [22]:

$$E_{eq}(\text{versus Hg/HgO}) = -0.9305 - 0.02955\log(P_{eq}) \quad \text{at } 293\,\text{K} \tag{1}$$

where the equilibrium potential (E_{eq}) was determined by alternately performing the following operation: (1) a pulse discharge of 10 mAh g^{-1} with 50 mA g^{-1} current density. (2) A rest period (about 20 min) for the potential to become constant. The high rate dischargeablity (HRD) was determined by examining the discharge capacity at various discharge current density and defined as the following equation:

$$\text{HRD} = \frac{C_d}{C_d + C_{100}} \times 100\% \tag{2}$$

where C_d is the discharge capacity at I_d current density and C_{100} is the residual discharge capacity at I_{100} current density after a alloy electrode is discharged at I_d current density.

To investigate the electrocatalytic activity and kinetics character of alloy electrodes, linear polarization, anodic polarization and hydrogen diffusion in alloy bulk were performed on CHI600A electrochemical workstation after alloy electrodes were activated. The linear polarization and anodic polarization were measured by scanning the electrode potential at a rate of 0.1 mV s^{-1} from −5 to 5 mV (versus open circuit potential) and 5 mV s^{-1} from open circuit potential to −0.45 V (versus Hg/HgO reference electrode), respectively, at 50% depth of discharge (DOD). The hydrogen diffusion was measured using the constant potential-step discharge technique. The full-charged electrodes were discharged at a constant potential-step of 0.6 V for more than 3000 s.

3. Result and discussion

3.1. Alloy structure

Fig. 1 shows the XRD patterns for different annealed alloys and Fig. 2 shows the Rietveld refinement patterns of $La_{0.67}Mg_{0.33}Ni_{2.5}Co_{0.5}$ alloy at 1123 and 1173 K annealing treatment. It can be seen that all of the alloys consisted of complex phases which can be identified as (La,

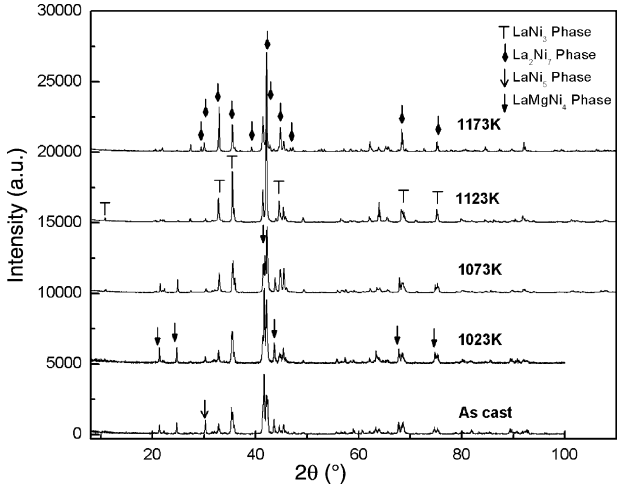

Fig. 1. XRD patterns for different annealed alloys.

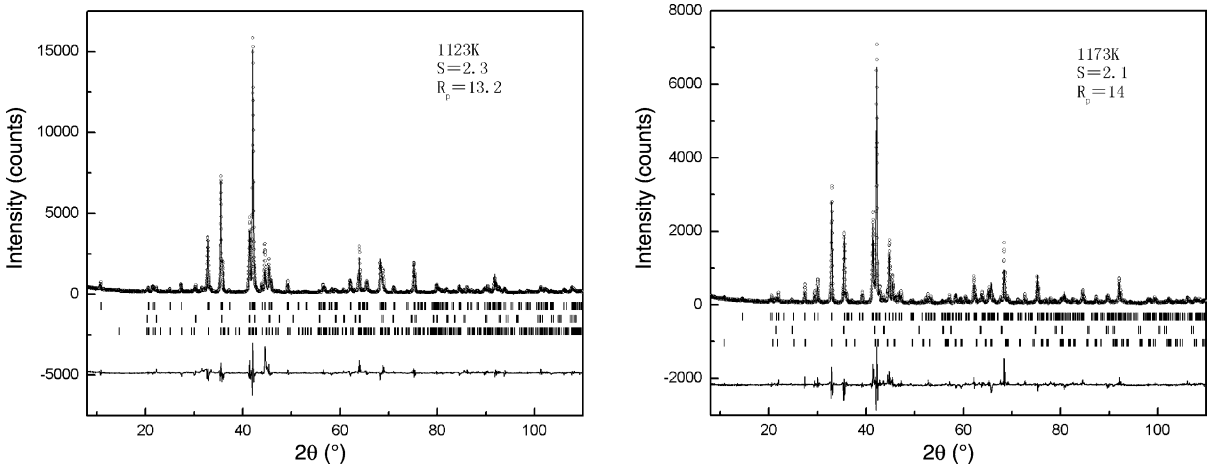

Fig. 2. Rietveld refinement patterns at 1123 and 1173 K for $La_{0.67}Mg_{0.33}Ni_{2.5}Co_{0.5}$ alloy.

Table 1
Characteristics of phases for different annealed alloys

Temperature (K)	Phase	Space group	Lattice constants (Å)				Phase abundance (wt.%)	Main phase real composition
			a	*c*	*V*	*c*/*a*		
As-cast	(La, Mg)(Ni, Co)$_3$	R- 3 m	5.046	24.345	536.812	4.82	49.10	$La_{0.67}Mg_{0.33}$(Ni, Co)$_3$
	La(Ni, Co)$_5$	P6/mmm	5.039	3.991	87.758	0.79	22.82	
	LaMg(Ni, Co)$_4$	F-4 3 m	7.186	7.186	371.075	1	28.08	
1023	(La, Mg)(Ni, Co)$_3$	R- 3 m	5.049	24.347	537.495	4.82	55.00	$La_{0.67}Mg_{0.33}$(Ni, Co)$_3$
	(La, Mg)$_2$(Ni, Co)$_7$	P6$_3$/mmc	5.047	24.206	533.959	4.80	8.94	
	LaMg(Ni, Co)$_4$	F-4 3 m	7.176	7.176	369.528	1	26.90	
	La(Ni, Co)$_5$	P6/mmm	5.036	3.991	87.654	0.79	9.16	
1073	(La, Mg)(Ni, Co)$_3$	R-3 m	5.048	24.340	537.127	4.82	68.65	$La_{0.67}Mg_{0.33}$(Ni, Co)$_3$
	(La, Mg)$_2$(Ni, Co)$_7$	P6$_3$/mmc	5.041	24.225	533.108	4.81	12.78	
	LaMg(Ni, Co)$_4$	F-4 3 m	7.175	7.175	369.370	1	14.53	
	La(Ni, Co)$_5$	P6/mmm	5.035	3.993	87.663	0.79	4.04	
1123	(La, Mg)(Ni, Co)$_3$	R-3 m	5.048	24.390	538.231	4.83	73.21	$La_{0.66}Mg_{0.34}$(Ni, Co)$_3$
	(La, Mg)$_2$(Ni, Co)$_7$	P6$_3$/mmc	5.051	24.237	535.490	4.80	22.24	
	La(Ni, Co)$_5$	P6/mmm	5.034	3.986	87.475	0.79	4.55	
1173	(La, Mg)$_2$(Ni, Co)$_7$	P6$_3$/mmc	5.046	24.252	534.761	4.81	92.50	$La_{1.50}Mg_{0.50}$(Ni, Co)$_7$
	LaMg(Ni, Co)$_4$	F-4 3 m	7.174	7.174	369.220	1	2.46	
	(La, Mg)(Ni, Co)$_3$	R-3 m	5.046	24.253	534.783	4.81	5.04	

Mg)(Ni, Co)$_3$ phase ($PuNi_3$-type, SG: R-3 m), (La, Mg)$_2$(Ni, Co)$_7$ phase (Ce_2Ni_7-type, SG: P6$_3$/mmc), LaMg(Ni, Co)$_4$ phase ($MgCu_4Sn$-type, SG: F-4 3 m) and La(Ni, Co)$_5$ phase ($CaCu_5$-type, SG:P6/mmm), respectively, by Rietveld analysis. Structure characteristics of different annealed alloys are tabulated in Table 1 and the evolution of phase abundance versus the annealing temperature are pictured in Fig. 3. It can be found that abundance of (La, Mg)$_2$(Ni, Co)$_7$ phase increased with rise of annealing temperature. What's more, (La, Mg)$_2$(Ni, Co)$_7$ phase became main phase (92.5 wt.%) at 1173 K. While abundance of (La, Mg)(Ni, Co)$_3$ phase increased from 49.10 wt.% (as-cast) to 73.21 wt.% (1123 K) firstly and then decreased to 5.04 wt.% dramatically at 1173 K. On the other hand, abundance of La(Ni, Co)$_5$ phase decreased from 22.82 wt.% (as-cast) to 4.04 wt.% (1123 K) with rise of annealing temperature and disappeared after 1123 K. At the same time, abundance of LaMg(Ni, Co)$_4$

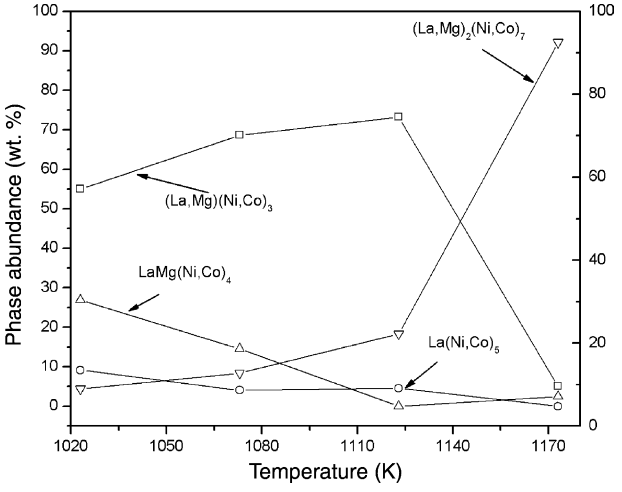

Fig. 3. Phase abundance variation curves for different annealed alloys.

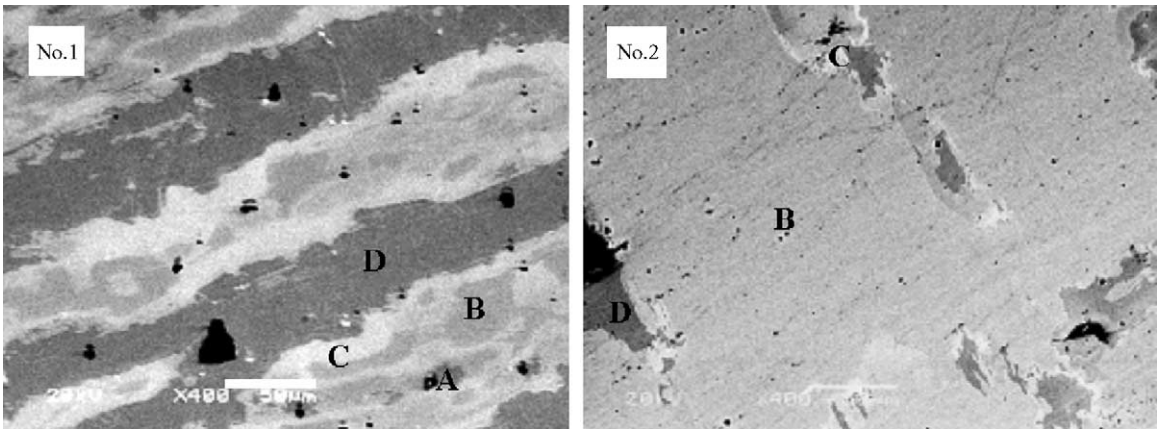

Fig. 4. Scattered electron images for different annealed alloys. No. 1 at 1023 K; No. 2 at 1173 K. A, B, C and D represent La(Ni, Co)$_5$ phase, (La, Mg)$_2$Ni$_7$ phase, (La, Mg)(Ni, Co)$_3$ phase and LaMg(Ni, Co)$_4$ phase, respectively.

phase also decreased with rise of annealing temperature and disappeared at 1123 K. However, at 1173 K, a little LaMg(Ni, Co)$_4$ phase appeared at 1173 K again. These experiment results show that annealing treatment at 1123 K benefited the formation of (La, Mg)(Ni, Co)$_3$ phase best. Below 1123 K, the composition of alloys was not very homogeneous just as shown in Fig. 4(No. 1) in which there are some La(Ni, Co)$_5$ phase, (La, Mg)$_2$(Ni, Co)$_7$ phase, (La, Mg)(Ni, Co)$_3$ phase and LaMg(Ni, Co)$_4$ phase. Presence of LaMg(Ni, Co)$_4$ phase and La(Ni, Co)$_5$ phase indicate that the peritectic reaction was not complete. However, at a higher temperature, the composition of alloys became homogeneous, except for small impurities, such as LaMg(Ni, Co)$_4$ phase and (La, Mg)(Ni, Co)$_3$ phase just like in Fig. 4(No. 2). It is worth noting that content of Mg element in alloys decreased with rise of annealing temperature due to volatilization of Mg element as shown in Fig. 5. From Fig. 5, it can be found that content of Mg at 1123 K was very similar to that of nominal alloy $La_{0.67}Mg_{0.33}Ni_{2.5}Co_{0.5}$, at the same time, the main phase in alloy was (La, Mg)(Ni, Co)$_3$. However, (La, Mg)$_2$(Ni, Co)$_7$

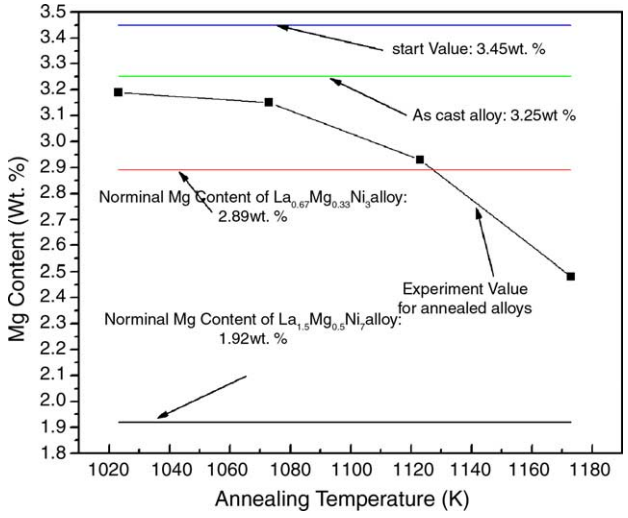

Fig. 5. Mg content variation curves for different annealed alloys.

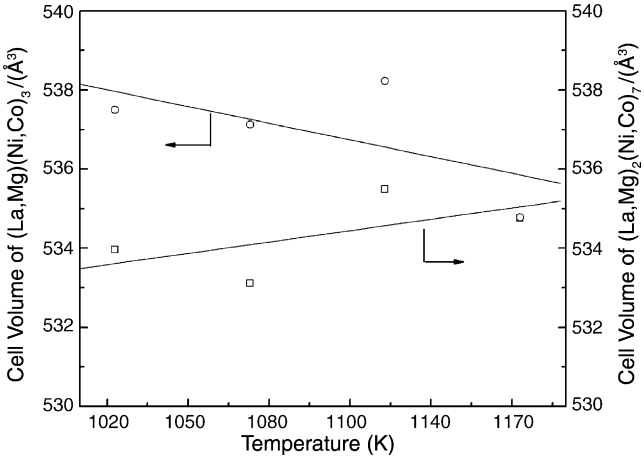

Fig. 6. Cell volume variation curves for different annealed alloys.

phase became main phase at 1173 K which could be attributed to volatilization of Mg element to some extent. But another detail is that content (2.48 wt.%) of Mg element in annealed alloy at 1173 K was much higher than that (1.92 wt.%) of $La_{1.5}Mg_{0.5}$(Ni, Co)$_7$ alloy, which implies that high temperature is in favor of formation of (La, Mg)$_2$(Ni, Co)$_7$ phase. From Table 1, it can be also found that Mg content of main phase in annealed alloys did not change obviously with the variation of annealing temperature, except for the annealed alloy at 1173 K. Small variation of cell volume supplied the proof from another aspect for above experiment result just as shown in Fig. 6. From Fig. 6, it can be noticed that cell volume of (La, Mg)(Ni, Co)$_3$ phase decreased and cell volume of $La_{1.5}Mg_{0.5}$(Ni, Co)$_7$ phase increased with rise of annealing temperature, but just a little. This result may be originated from the distribution of Co element in every phase of alloy with rise of annealing temperature.

3.2. Thermodynamic characteristics

Fig. 7 shows the electrochemical desorption *P–C* isotherm for different annealed alloys, and Table 2 summarizes the

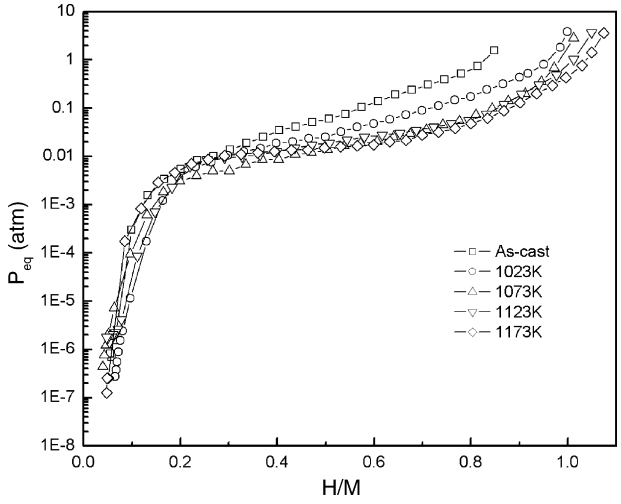

Fig. 7. Electrochemical desorption *P–C* isotherms for different annealed alloy electrodes at 293 K.

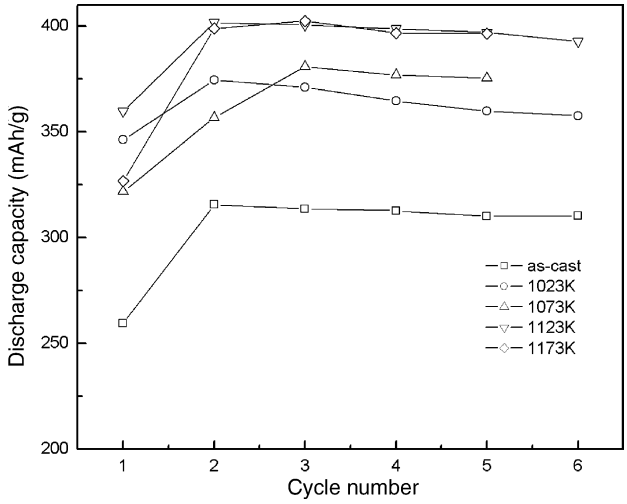

Fig. 8. Activation curves of different annealed alloy electrodes with 100 mA g^{-1} charge–discharge current density at 293 K.

absorption/desorption characteristics of different alloys. It can be seen that the desorption plateau became flatter and wider little by little with rise of annealing temperature, which could be related with homogenization of alloy composition. From Table 2, it is obvious that the hysteresis factor was small and ranged between 0.187 and 0.332, that the plateau slope decreased from 1.434 (as-cast) to 0.755 (1173 K) with rise of annealing temperature. In addition, the hydrogen content (H/M) also increased with rise of annealing temperature and reached maximum (1.06 H/M) at 1173 K, which could be attributed to the decrease of $LaMg(Ni, Co)_4$ phase and $(LaNi, Co)_5$ phase. It should be noticed that the hydrogen content between 1123 and 1173 K annealed alloy was very near, which means that hydrogen content of $La_{1.5}Mg_{0.5}(Ni, Co)_7$ alloy is very similar to that of $(La, Mg)(Ni, Co)_3$ alloy.

3.3. Charge/discharge characteristics

Fig. 8 shows the activation curves of different alloy electrodes, and Table 3 summarizes electrochemical performance of different alloy electrodes. It can be found that all of the alloy electrodes exhibited good activation properties; three times of charge/discharge cycles were enough to activate electrodes. The maximal discharge capacity increased from 315.64 mAh g^{-1} (as-cast) to 402.50 mAh g^{-1} (1173 K) with rise of annealing temperature, which may be due to the decrease of $LaMg(Ni, Co)_4$ and $La(Ni, Co)_5$ phase, $LaMgNi_4$ alloy electrode exhibited low discharge capacity and poor cyclic stability [23].

Fig. 9 shows the cyclic stability curves of different annealed alloy electrodes. It can be found that cyclic stabil-

Table 2
Hydrogen absorption/desorption characteristics for different annealed alloys

Temperature (K)	H/M	P_a (atm)	P_d (atm)	Hysteresis factor log (P_a/P_d)	Plateau slope[a]
As-cast	0.85	0.101	0.053	0.280	1.434
1023	1.00	0.054	0.026	0.317	1.263
1073	1.01	0.020	0.013	0.187	1.048
1123	1.05	0.043	0.020	0.332	0.795
1173	1.06	0.027	0.015	0.255	0.755

P_a is the pressure at midpoint of absorption hydrogen process; P_d is the pressure at midpoint of desorption hydrogen process.
[a] Plateau slope = $\log(p|x(H)/x(M) = 0.75/P|x(H)/x(M) = 0.25)$.

Table 3
Summary of electrochemical performance for different annealed alloy electrodes at 293 K

Temperature (K)	N	C_{max} (mAh g^{-1})	HRD_{900} (%)	S_{70} (%)	I_0 (mA g^{-1})	I_L (mA g^{-1})	D ($\times 10^{-10}$ cm^2 s^{-1})
As-cast	2	315.64	68.73	69.8	143.08	1400	3.49
1023	2	374.60	73.62	66.5	181.59	1440	3.54
1073	3	380.84	71.98	67.7	176.45	1410	3.15
1123	2	401.78	61.03	71.7	211.46	1750	2.02
1173	3	402.50	87.72	92.9	226.87	2170	3.62

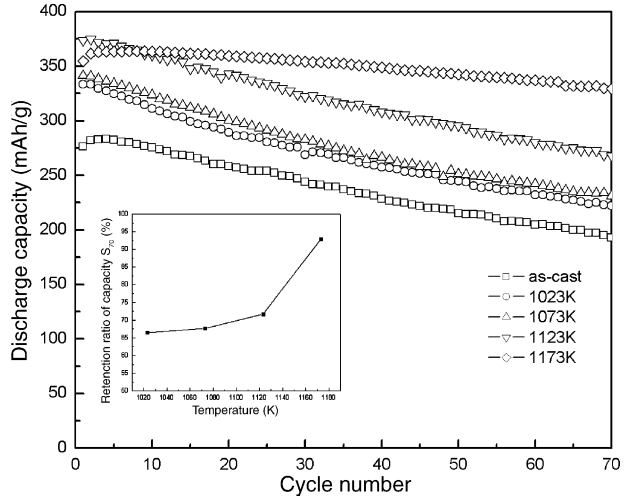

Fig. 9. Cyclic stability curves of different annealed alloy electrodes with 300 mA g^{-1} charge–discharge current density at 293 K.

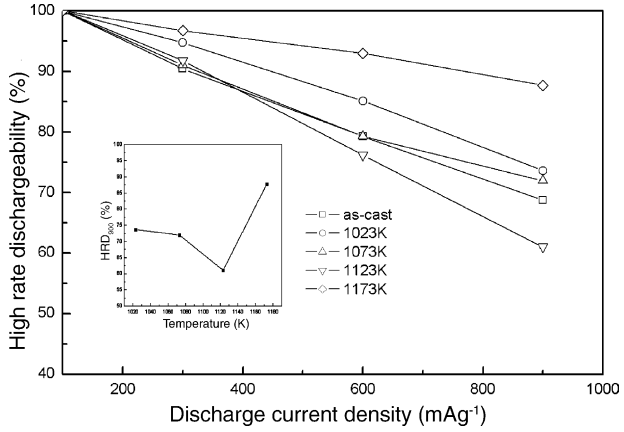

Fig. 10. High rate dischargeability (HRD) curves of different annealed alloy electrodes at 293 K.

ity was improved obviously from 69.8% (as-cast) to 92.9% (1173 K) by annealing treatment, which could be attributed to the phase evolution in alloys. It should be noticed that the cycle stability was improved dramatically at 1173 K. At the same time, the main phase was $La_{1.5}Mg_{0.5}(Ni, Co)_7$ phase (92.9 wt.%) at 1173 K. The experiment phenomenon indicates that cyclic stability of $(La, Mg)_2(Ni, Co)_7$ phase is much better than that of (La, Mg)$(Ni, Co)_3$ phase. From Fig. 3, it can be concluded that decrease of $LaMg(Ni, Co)_4$ phase abundance and increase of $La_{1.5}Mg_{0.5}(Ni, Co)_7$ phase abundance are important factors to improve cycle stability of annealing alloy electrodes. It is well known that the degradation of discharge capacity for alloy electrodes can be influenced mainly by two factors: surface passivation of alloy electrodes because of oxidation of active composition and pulverization of alloy particles due to cell volume expansion in hydrogen absorption/desorption process [5]. In this paper, the latter seems to be more important to influence cyclic stability of alloy electrodes since all alloys contained the same component elements. However, the only difference between different annealed alloys was the different phase structure. Therefore, the much better cyclic stability of $(La, Mg)_2(Ni, Co)_7$ alloy electrodes than that of (La, Mg)$(Ni, Co)_3$ alloy electrodes may be originated from the crystal structure difference of alloys and hydrides. An in-depth study is going on in our laboratory.

3.4. Electrochemical kinetic characteristics

Fig. 10 shows the high rate dischargeability curves of different alloy electrodes. It can be found that annealing treatment improved the HRD characteristic from 68.73% (HRD_{900}, as-cast) to 73.02% (HRD_{900}, 1023 K). However, with the annealing temperature rise further, HRD_{900} decreased gradually from 73.02% (1023 K) to 61.03% (1123 K), which means that HRD characteristic of (La, Mg)$(Ni, Co)_3$ alloy electrode is not good since (La, Mg)$(Ni, Co)_3$ phase in alloys increased with the rise of annealing temperature. However, it was excited that HRD_{900} at 1173 K increased to 87.72% suddenly, which could be attributed to the appearance of main phase $(La, Mg)_2(Ni, Co)_7$. The experiment result shows that kinetic characteristic of $(La, Mg)_2(Ni, Co)_7$ phase is much better than that of (La, Mg)$(Ni, Co)_3$ phase. It is known that HRD characteristic stands for overall kinetic properties, HRD can be influenced mainly by charge transfer on surface of alloy electrodes and hydrogen diffusion in alloy bulk. Table 3 summarized the kinetic characteristics of alloy electrodes. Exchange current density (I_0) can be calculated according to the following equation [24]:

$$I_0 = \frac{RTI_d}{F\eta} \tag{3}$$

where R is the gas constant, T the absolute temperature, I_d the applied current density, F the Faraday constant and η is the total overpotential. It is known that exchange current density (I_0) and limiting current density (I_L) are the other parameters to describe the kinetic characteristic of alloy electrodes. I_0 can be used to judge the speed of charge transfer on surface of alloy electrodes. I_L can be influenced by charge transfer, hydrogen diffusion and passivation of active composition. As shown in Table 3, I_0 increased from 143.08 mA g^{-1} (as-cast) to 226.87 mA g^{-1} (1173 K) and I_L increased from 1400 mA g^{-1} (as-cast) to 2170 mA g^{-1} (1173 K); however, the order of I_0 and I_L was reverse to that of HRD from 1023 K to 1123 K, which indicate that hydrogen reaction on surface of alloy electrodes was not the control process. At the same time, alloy electrodes with main phase $(La, Mg)_2(Ni, Co)_7$ exhibited the largest value of I_0 and I_L.

Fig. 11 shows the semilograrithmic plots of anodic current versus time responses of different alloy electrodes at full-charged state and 293 K. Hydrogen diffusion coefficient (D) can be attained according to the following equation [25]:

$$\log(i) = \log\left(\frac{6FD(C_0 - C_s)}{da^2}\right) - \left(\frac{\pi^2}{2.303}\right)\left(\frac{D}{a^2}\right)t \tag{4}$$

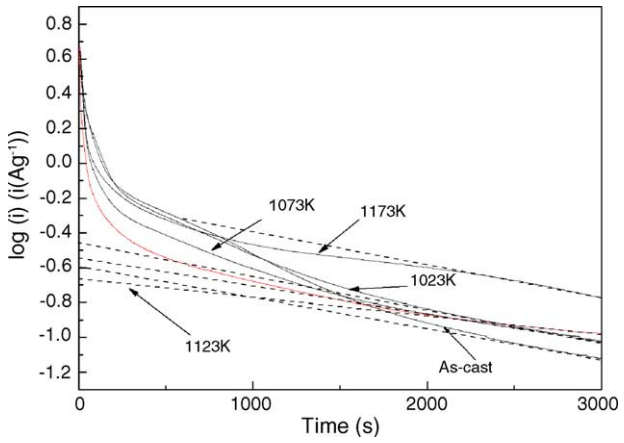

Fig. 11. Semilogarithmic plots of anodic current vs. time responses of different alloy electrodes at full-charged state and 293 K.

where D, C_0, C_s, a, d, t and i are the hydrogen diffusion coefficient ($cm^2\ s^{-1}$), the initial hydrogen concentration in the bulk of the alloy (mol cm^{-3}) the hydrogen concentration on the surface of the alloy particles (mol cm^{-3}), the alloy particle radius (cm), the density of the hydrogen storage alloy (g cm^{-3}), the discharge time (s) and the diffusion current density (A g^{-1}), respectively. So according to the slope of log(i) versus t, D can be calculated. Value of D is also listed in Table 3, it can be seen that the order of D value is consistent with that of HRD_{900} value basically, which implies that hydrogen diffusion in alloy bulk is more important factor than hydrogen reaction on surface of alloy electrodes. At the same time, the alloy electrode with main phase (La, $Mg)_2$(Ni, $Co)_7$ exhibited the best hydrogen diffusion characteristic, however, the alloy with main phase (La, Mg)Ni_3 exhibited the small hydrogen diffusion, which indicates that (La, $Mg)_2$(Ni, $Co)_7$ alloys possess much better kinetic characteristic than that of (La, Mg)Ni_3 alloys in hydrogen absorption/desorption process.

4. Conclusion

The structure and electrochemical properties of different anneal alloys have been studied systematically. Some conclusions can be summarized:

(1) Annealing treatment had an important influence on phase structure of alloys. All alloys consisted of complex phase such as (La, Mg)(Ni, $Co)_3$ phase, (La, $Mg)_2$(Ni, $Co)_7$ phase, LaMg(Ni, $Co)_4$ phase and La(Ni, $Co)_5$ phase. Annealing treatment at 1123 K benefited formation of (La, Mg)(Ni, $Co)_3$ phase best and annealing treatment at 1173 K was in favor of formation of (La, $Mg)_2$(Ni, $Co)_7$ phase. (La, $Mg)_2$(Ni, $Co)_7$ phase became the main phase (92.5 wt.%) when the temperature of annealing treatment was 1173 K. Annealing treatment had not influenced nearly on the lattice parameters of every phase. Annealing treatment at high temperature could lead to volatility of Mg element.

(2) With the rise of annealing temperature, hydrogen absorption/desorption plateau became flatter and wider. The maximal discharge capacity (C_{max}) of alloy electrodes increased from 315.64 mAh g^{-1} (as-cast) to 402.50 mAh g^{-1} (1173 K). All of the alloy electrodes can be activated easily by three charge/discharge cycles. High rate dischargeability was deteriorated as (La, Mg)(Ni, $Co)_3$ phase increased, alloy electrode with main phase (La, $Mg)_2$(Ni, $Co)_7$ exhibited the best HRD characteristic. Hydrogen reaction on alloy electrodes surface of (La, Mg)(Ni, $Co)_3$ alloy was not the control process of electrode reaction, hydrogen diffusion in alloy bulk was a more important factor influencing kinetic characteristics of alloy electrodes. In addition, alloy electrode with main phase (La, $Mg)_2$(Ni, $Co)_7$ exhibited largest value of exchange current density, limiting current density and hydrogen diffusion coefficient.

(3) Then a conclusion can be made that (La, $Mg)_2$(Ni, $Co)_7$ alloy electrodes possess much better overall electrochemical properties than (La, Mg)(Ni, $Co)_3$ alloy electrodes. (La, $Mg)_2$(Ni, $Co)_7$ alloy with Ce_2Ni_7-type structure is very potential as new type negative materials of Ni/MH secondary cell.

Acknowledgement

This work was supported by the National Nature Science Foundation of China (No. 50171021).

References

[1] C.-J. WinterInt, J. Hydrogen Energy 29 (2004) 1095–1097.
[2] T. Sakai, M. MatsuoKa, C. Iwakura, in: L. Eyring (Ed.), Handbook on the Physics and Chemistry of Rare Earths, Elesvier, Amsterdam, 1995, p. 133.
[3] F. Feng, M. Geng, D.O. Northwood, Int. J. Hydrogen Energy 26 (2001) 725–734.
[4] G. Sandrock, J. Alloys Compd. 293–295 (1999) 877–888.
[5] J.J. Reilly, Metal hydrides electrode, in: J.O. Besenhard (Ed.), Handbook of Battery Materials, Wiley, New York, 2000.
[6] K. kadir, T. Sakai, I. Uehara, J. Alloys Compd. 302 (2000) 112–117.
[7] H. Pan, Y. Liu, M. Gao, Y. Lei, Q. Wang, J. Electrochem. Soc. 150 (5) (2003) A565–A570.
[8] J. Chen, N. Kuriyama, H.T. Takashita, H. Tanada, T. Sakai, M. Haruta, Electrochem. Solid State Lett. 3 (6) (2000) 249–252.
[9] R. Tang, Z. Zhang, L. Liu, Y. Liu, J. Zhu, G. Yu, Int. J. Hydrogen Energy 29 (2004) 851–858.
[10] B. Liao, Y.Q. Lei, L.X. Chen, G.L. Lu, H.G. Pan, Q.D. Wang, J. Power Sources 129 (2004) 358–367.
[11] Y. Liu, H. Pan, M. Gao, R. Li, Y. Lei, J. Alloys Compd. 376 (2004) 296–303.
[12] T. Kohno, H. Yoshida, M. Kanda, J. Alloys Compd. 363 (2004) 249–252.
[13] B. Liao, Y.Q. Lei, L.X. Chen, G.L. Lu, H.G. Pan, Q.D. Wang, J. Alloys Compd. 376 (2004) 186–195.
[14] H. Pan, Q. Jin, M. Gao, Y. Liu, R. Li, Y. Lei, Q. Wang, J. Alloys Compd. 376 (2004) 196–204.

[15] B. Liao, Y.Q. Lei, L.X. Chen, G.L. Lu, H.G. Pan, Q.D. Wang, Electrochim. Acta 50 (2004) 1057–1063.
[16] Y. Liu, H. Pan, M. Gao, Y. Zhu, L. Yongquan, J. Alloys Compd. 365 (2004) 246–252.
[17] H. Pan, Y. Liu, M. Gao, Y. Zhu, Y. Lei, Q. Wang, Int. J. Hydrogen Energy 28 (2003) 113–117.
[18] T. Kohno, H. Yoshida, F. Kawashima, T. Inaba, I. Sakai, M. Yamamoto, M. Kanda, J. Alloys Compd. 311 (2000) L5–L7.
[19] R.A. Young, in: R.A. Roung (Ed.), Introduction to the Rietveld Method, Oxford University Press Inc., New York, 1995, pp. 1–38.
[20] J. Rodriguez-Carvajal, in: Abstract of the Satellite Meeting on Powder Diffraction, Congress of IUCr, Toulouse, France, P127(1990); Fullprof Program, Version 3.5d October 98-LLB-JRC,1998.
[21] N. Cui, J.L. Luo, Electrochim. Acta 45 (2000) 3973–3981.
[22] J. Balej, Int. J. Hydrogen Energy 10 (1985) 365–374.
[23] Z.M. Wang, H.Y. Zhou, Z.F. Gu, G. Cheng, A.B. Yu, J. Alloys Compd. 377 (2004) L7–L9.
[24] P.H.L. Notten, P. Hokkeling, J. Electrochem. Soc. 138 (1991) 1877–1885.
[25] G. Zheng, B.N. Popov, R.E. White, J. Electrochem. Soc. 142 (1995) 2695–2698.